Progress In Electromagnetics Research C, Vol. 134, 65–77, 2023

Complete Design Procedure of a Size Constrained Printed Planar Log-Periodic Dipole Antenna

Guilherme C. Vieira and Custódio Peixeiro*

Abstract—This paper describes the design, fabrication, and test of a printed planar log-periodic dipole antenna to be used as a standard gain antenna in simple, low frequency, anechoic chamber far-field antenna measurements. The design procedure is size constrained by the photolithographic printing circuit fabrication process. Maximum gain and an input reflection coefficient below −10 dB are envisaged for the frequency range 0.5–2.5 GHz. The antenna is printed on a low cost FR4 substrate, and a careful analysis, with optimization of all the antenna physical parameters namely: number, length, spacing and width of the dipoles, width of the feed line traces, feed line termination, feed balun, and substrate shape, is carried out. The good agreement obtained between numerical simulation and experimental results provides validation of the proposed antenna configuration and design procedure.

1. INTRODUCTION

Since its invention by Isbell [1], in 1959, and the introduction of simple design rules by Carrel [2], in 1961, log-periodic dipole antenna (LPDA) has been successfully used in many civil and military applications ranging from the high frequency (HF) band [3] to millimeter waves [4, 5]. There is a wide variety of such applications, namely: HF ionospheric communications [3, 6], TV reception [7], satellite communication systems [8], Wi-Fi [9], ultra-wideband (UWB) communications [10], 5G communication systems [11], electromagnetic compatibility (EMC)/electromagnetic interference (EMI) measurements [12–14], radio frequency identification (RFID) [15], direction finding [16, 17], measurement of the macroscopic characteristics of building materials [18], automotive radar [5], wireless energy harvesting [19], mm-wave passive imaging systems [4], electrical field sensors [20], and radio astronomy [13, 21, 22]. Its continued success stems from the extremely wide bandwidth (conceptually unlimited, in practice only constrained by size at low frequencies and fabrication accuracy at high frequencies), stable unidirectional radiation pattern, medium gain, very low cross polarization, and simple easy to design low profile geometry. For frequencies up to the very high frequency (VHF) band only wire dipoles can be used, but for the ultra-high frequency (UHF) band and above, printed configurations are usually adopted combining the advantages of the LPDA and of the photolithographic printing circuit board (PCB) technology [23].

The University of Lisbon far-field anechoic chamber ($8 \times 4 \times 4\,\mathrm{m}^3$) facility is certified for antenna measurements above 2 GHz. A set of pyramidal horns from Flan Microwave (FMi) [24] are used as standard gain antennas. Mostly for academic work (MSc and PhD thesis) but also for some industrial and research projects there is the need of experimental validation of new antenna concepts and configurations, below 2 GHz. Although such experimental results cannot be certified they, submitted to an appropriate critical analysis, can be valuable. Standard gain horns to be used below 2 GHz are expensive, bulky, heavy, and difficult to handle. For instance, the FMi horn for the frequency band 1.14–1.73 GHz (model no. 06240-10), with the corresponding waveguide to coaxial transformer, weights 12.9 kg and is 64.5 cm long. On the contrary, a printed planar LPDA is low cost, low profile, lightweight,

Received 20 April 2023, Accepted 12 June 2023, Scheduled 28 June 2023
* Corresponding author: Custódio Peixeiro (custodio.peixeiro@lx.it.pt).
The authors are with the Instituto de Telecomunicações, Instituto Superior Técnico, University of Lisbon, Portugal.

and easy to handle. Moreover, it can cover the frequency range of several pyramidal horns avoiding the cumbersome and time-consuming change of the standard gain antenna in wideband measurements.

This paper describes the design, fabrication, and test of a printed planar log-periodic dipole antenna to be used, in this facility, as a standard gain antenna in the frequency range 0.5–2.5 GHz. The design is size constrained by the maximum PCB allowed ($420 \times 350\,\text{mm}^2$) in the photolithographic printed circuit fabrication process. This constraint imposes a limitation to the antenna width and length. The physical parameters of the size constrained LPDA configuration are optimized to provide an input reflection coefficient below -10 dB in the 50 Ohm coaxial feed cable, and maximal gain, in the indicated frequency range. There are many printed LPDAs available commercially, the novelty of the proposed approach comes from the size constraints and the optimization of each of the antenna physical parameters to fulfil the requirements of the envisaged application as standard gain antenna in far-field anechoic chamber low-frequency wideband antenna measurements. Moreover, it is necessary to point out that a new and complete iterative design procedure is used to fulfill the imposed size constraints while maximizing the gain. Such gain maximization is important to mitigate the effects of unwanted reflections on the anechoic chamber walls.

2. ANTENNA CONFIGURATION

The printed planar LPDA geometry is shown in Fig. 1. This antenna is printed on a substrate with relative electric permittivity ε_r, loss tangent $\tan\delta$, and thickness h.

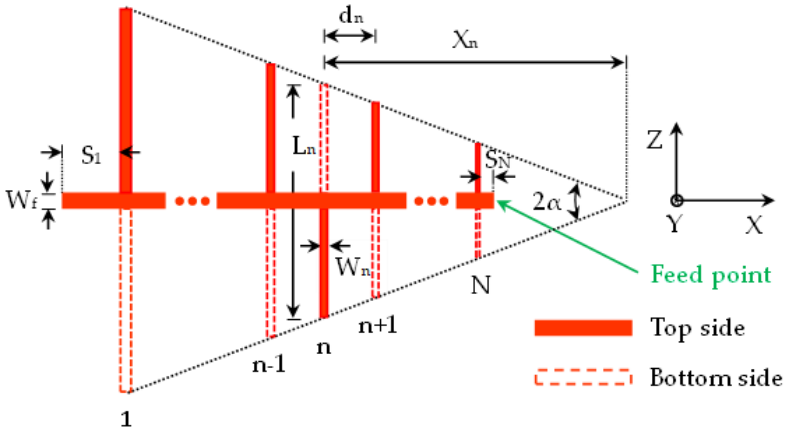

Figure 1. Geometry of the printed planar LPDA.

The scaling factor (τ) and spacing factor (σ) are defined as [1, 2]

$$\tau = \frac{L_{n+1}}{L_n} = \frac{d_{n+1}}{d_n} = \frac{W_{n+1}}{W_n} = \frac{X_{n+1}}{X_n} \quad 1 \le n \le N \tag{1}$$

$$\sigma = \frac{d_n}{2L_n} \tag{2}$$

The apex angle (2α), the number of dipoles (N), and the antenna total length (L_A) are obtained from

$$\tan\alpha = \frac{L_n}{2X_n} = \frac{L_n - L_{n+1}}{2d_n} = \frac{1-\tau}{4\sigma} \tag{3}$$

$$N = 1 + \frac{\log\left(L_1/L_N\right)}{\log\left(1/\tau\right)} \tag{4}$$

$$L_A = (X_1 - X_N) + \frac{W_1}{2} + \frac{W_N}{2} + S_1 + S_N \tag{5}$$

The geometry of the printed LPDA is defined when the parameters τ, σ, L_1 (or L_N), N, W_1 (or W_N), W_f, S_1, and S_N are specified, together with the substrate. All these parameters are optimized in the proposed design procedure.

The antenna is fed by a semi-rigid miniature 50 Ω coaxial cable near the shortest dipole. As the antenna radiation pattern points toward the apex (end-fire array) and to avoid interference of the cable and distortion of the radiation pattern, the cable runs towards the antenna apex along the top side of the feeding transmission line and is connected to it by a simple balun. This balun consists in connecting the outer conductor of the cable to the top strip of the feeding line and the inner conductor of the cable to the bottom strip using a via-hole in the substrate [10].

3. ANTENNA DESIGN AND OPTIMIZATION

3.1. Antenna Design First Iteration

The design procedure follows the steps introduced in [2] with the corrections provided in [25]. As the printed LPDA is dielectrically inhomogeneous, the definition of the equivalent homogenous structure requires the calculation of the effective relative electric permittivity (ε_{ref}). However, different dipoles have different widths, and there is not a straightforward way to calculate ε_{ref} accurately. Therefore, initially a free space antenna is designed to serve as a reference (1st iteration). Later, the presence of the substrate will be taken into account, and the LPDA parameters optimized to fulfil the specifications.

The (τ, σ) pair is chosen from the directivity (D) plots. These plots are given for $8 \leq D$ (in dB) ≤ 13. As a larger directivity leads to a longer antenna, an initial directivity goal of 8 dB was chosen. The corresponding optimum (τ, σ) pair is $\tau = 0.857$ and $\sigma = 0.166$ [25]. L_1 and L_N are obtained from $\lambda_{\max}$, $\lambda_{\min}$, and the truncation coefficients K_1 and K_2 as

$$L_1 \geq K_1 \lambda_{\max} \tag{6}$$

$$L_N \leq K_2 \lambda_{\min} \tag{7}$$

leading to $L_1 = 332.0$ mm ($L_N = 44.7$ mm). From Equations (3) to (5) we obtain $\alpha = 12.15°$, $N = 14$, and $L_A = 675.1$ mm. For $W_1 = 14.0$ mm, $W_f = 2.2$ mm, $S_1 = S_N = 0$, this LPDA, printed on an FR4 substrate ($\varepsilon_r = 4.3$, $h = 1.6$ mm, $\tan\delta = 0.025$ and metallization thickness 35 µm), was simulated in CST Studio Suite [26]. The $|S_{11}|$ results obtained are shown in Fig. 2.

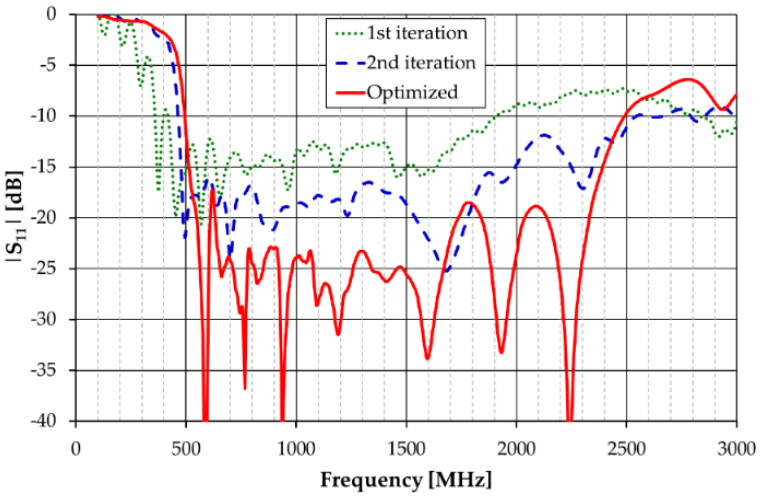

Figure 2. Evolution of the $|S_{11}|$ simulated results.

As can be concluded and as expected, the low frequency point (f_1) where $|S_{11}| = -10$ dB is significantly below the required lowest frequency of operation (500 MHz), meaning that the longest dipole is too long. This situation affects not only the low and high frequency limits but also the total antenna length.

3.2. Longest Dipole Length (L_1)

Using a trial-and-error procedure in CST simulations, the length of the first dipole $L_1 = 250.0\,\text{mm}$ ($L_N = 33.6\,\text{mm}$) was obtained corresponding to an f_1 of approximately 500 MHz. As all the other parameters (τ, σ, N, W_1, W_f, S_1 and S_N) were kept unchanged, the total antenna length $L_A = 510.3\,\text{mm}$ was obtained. This value of L_A is still larger than the maximum allowed ($L_{A\,\text{max}} = 420\,\text{mm}$). However, it is now clear that the width of the PCB is not a problem since L_1 is 100 mm less than the maximum. The corresponding CST $|S_{11}|$ simulation results are also shown in Fig. 2 (curve labelled "2nd iteration"). As can be verified, the $|S_{11}|$ specifications are fully accomplished ($|S_{11}| \leq -10\,\text{dB}$ in the frequency range 464.2–2544.3 MHz). However, the antenna is still too long. Therefore, the (τ, σ) pair and the number of dipoles (N) must be modified to fulfil the specifications and meet the maximum antenna length restriction.

3.3. Termination Stub (S_1)

By reflecting the energy (travelling in the feeding line towards the region of longer dipoles) not radiated by the antenna back to it, the length of the termination stub (S_1) can be used to optimize the antenna performance in the lower part of the frequency band of operation. Either open or short-circuit stubs can be used. In this specific case, where the antenna length needs to be minimized, the best solution is the open stub with $S_1 = 0$.

3.4. Scaling and Spacing Factors (τ, σ) and Number of Dipoles (N)

Increasing the number of dipoles (N) will not affect f_1 and will produce the necessary increase of the high frequency limit (f_2) until it reaches 2500 MHz. However, this will also increase L_A which is already above the limit. Therefore, according to Equations (5) and (3), to decrease L_A, the spacing factor (σ) needs to be decreased. Moreover, by increasing the scaling factor (τ) and the number of dipoles there is an improvement of the gain. The best $|S_{11}|$ and gain performance was obtained for $\tau = 0.89$, $\sigma = 0.11$, and $N = 17$. An antenna length $L_A = 429.5\,\text{mm}$ is now obtained.

3.5. Feed Line Width (W_f)

Having chosen the substrate (ε_r, h), the width of the feed line strips (W_f) defines the characteristic impedance of the feeding transmission line. It was found that $W_f = 3.7\,\text{mm}$ was the best choice to match the 50 Ω coaxial cable. However, to have the same current on the top and bottom strips of the

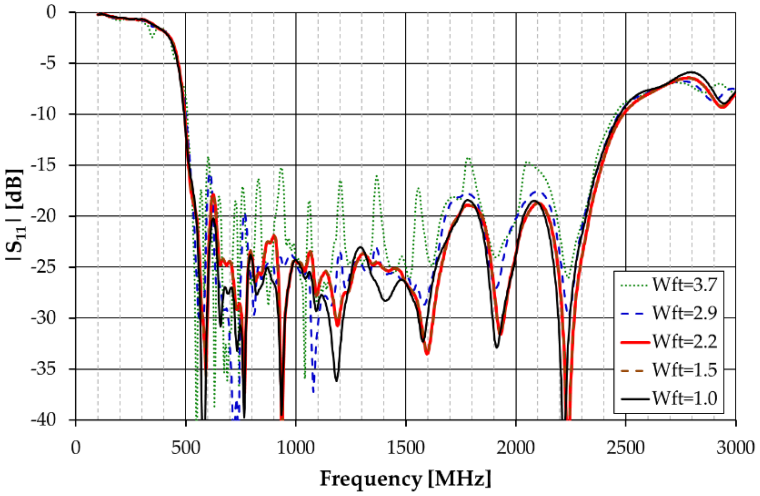

Figure 3. Effects of the feed top strip width (W_{ft}) on the input reflection coefficient.

feed transmission line, the top strip width (W_{ft}) needs to be decreased to account for the loading effect of the coaxial cable [27, 28]. The best balance for $W_{fb} = 3.7\,\text{mm}$ is $W_{ft} = 2.2\,\text{mm}$, as shown in Fig. 3 ($|S_{11}|$) and Fig. 4 (gain). However, the effects of W_{ft} on both $|S_{11}|$ and gain are moderate. Although $W_{ft} = 2.2\,\text{mm}$ and $W_{ft} = 1.5\,\text{mm}$ provide almost identical results, $W_{ft} = 2.2\,\text{mm}$ is chosen because it leads to a more reliable PCB etching process.

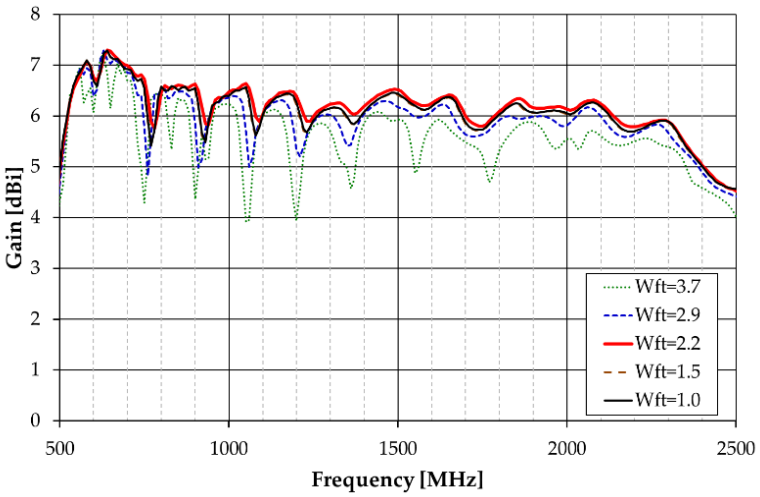

Figure 4. Effects of the feed top strip width (W_{ft}) on the gain.

3.6. Other Parameters

The dipoles' width and the substrate shape also affect the antenna performance. However, their effects are not significant. Concerning the dipoles' width, $W_N = 1\,\text{mm}$ was imposed, and the other widths were obtained applying the scaling factor. A trapezoidal shape configuration was obtained by truncating the substrate with a 40 mm margin from the end of each dipole.

3.7. Final Optimized Antenna

Since the antenna is size constrained, the antenna physical parameters cannot be optimized freely. Moreover, except the dipoles' lengths and the scaling and spacings factors pair (τ, σ), all the other parameters (termination stub length, feed line widths, dipoles' widths, and substrate shape and size) have a moderate effect on the antenna performance. However, although the effects of each of these parameters are moderate, the combined effects can be quite significant. Therefore, each of the antenna physical parameters has been individually optimized, as described above. After that, there was a small refinement of the longest dipole length (L_1). The LPDA with the highest gain that fulfils the impedance bandwidth requirements and meets the size restrictions corresponds to the following physical parameters: $\tau = 0.89$, $\sigma = 0.11$, $L_1 = 245.0\,\text{mm}$ ($L_{17} = 38.0\,\text{mm}$), $N = 17$, $W_{ft} = 2.2\,\text{mm}$, $W_{fb} = 3.7\,\text{mm}$, $W_{17} = 1.0\,\text{mm}$ ($W_1 = 6.5\,\text{mm}$), $S_1 = S_N = 0$. The corresponding antenna length is $L_A = 417.8\,\text{mm}$, and the dimensions of the sides of the trapezoidal substrate are 325.0 mm and 118.0 mm. A 1.1 mm margin from the antenna maximum length was used on both the longest and shortest dipole region to make sure that the substrate cutting did not damage the dipoles' metallization.

There are many systematic procedures proposed in the literature to optimize LPDAs [21, 29–31]. However, they do not consider all the antenna parameters taken into account in this work, and they do not provide physical insight of the radiation mechanisms.

The $|S_{11}|$ CST simulation results obtained for the optimized LPDA are shown in Fig. 2 (curve labelled "Optimized"). As can be seen $|S_{11}| \leq -10\,\text{dB}$ in the whole frequency range of interest (500–2500 MHz). The corresponding far-field E-plane (XZ) and H-plane (XY) cuts radiation pattern CST simulation results are shown in Fig. 5. It can be verified that the shape of the radiation pattern is stable

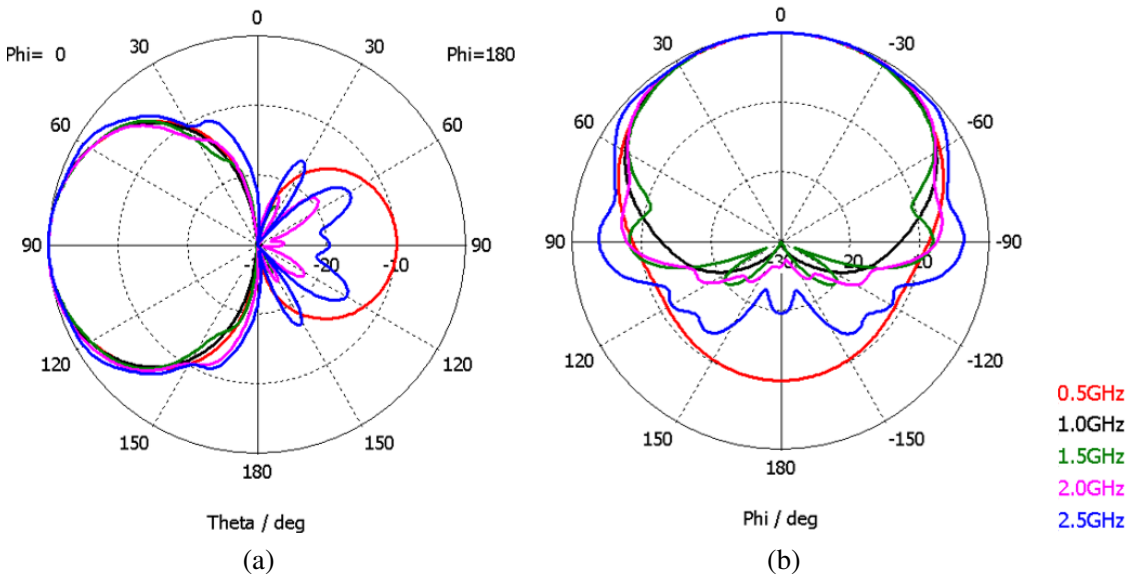

Figure 5. Radiation pattern simulated results of the optimized LPDA. (a) E-plane; (b) H-plane.

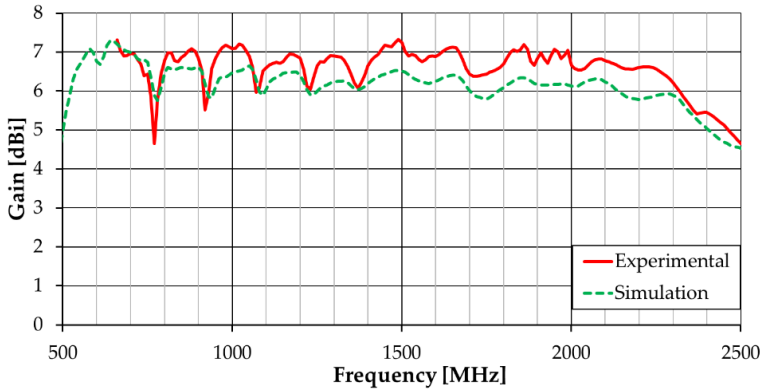

Figure 6. Comparison of simulation and experimental realized gain results.

in the frequency range of operation except for 500 MHz where a significant back radiation occurs. This is common since in this frequency the active region is composed of the longest dipoles. However, the front lobe is almost the same for the whole frequency band of operation.

The CST simulated gain versus frequency is shown in Fig. 6. The typical log-periodic behavior is observed. Some asymmetries (around 770 MHz, for instance) caused by resonance phenomena can also be observed [32–36]. A gain span in the range 4.6–7.3 dBi with an average of 6.1 dBi is obtained. The gain drops near the limits of the frequency band of operation since the active region contains less dipoles there [2, 25], as can be confirmed in the current distribution shown in Fig. 7. This is a consequence of the design criteria that favor compactness. The gain could be increased but at the expenses of other characteristics, such as polarization purity [37].

The efficiency (radiation and total) is shown in Fig. 8. The efficiency spans the range -1.8 dB to -1.0 dB with an average of -1.4 dB (72%). Therefore, the average directivity is 7.5 dB which corroborates the initial 8 dB goal.

The discrimination of the radiation pattern in the orthogonal polarization components E_θ and E_φ is shown in Fig. 9. The polarization purity of the antenna is confirmed, as the E_φ component is, at least, 30 dB below the E_θ component. This remarkably high polarization purity is essential for the envisaged application as a standard antenna for anechoic chamber far-field measurements, where the

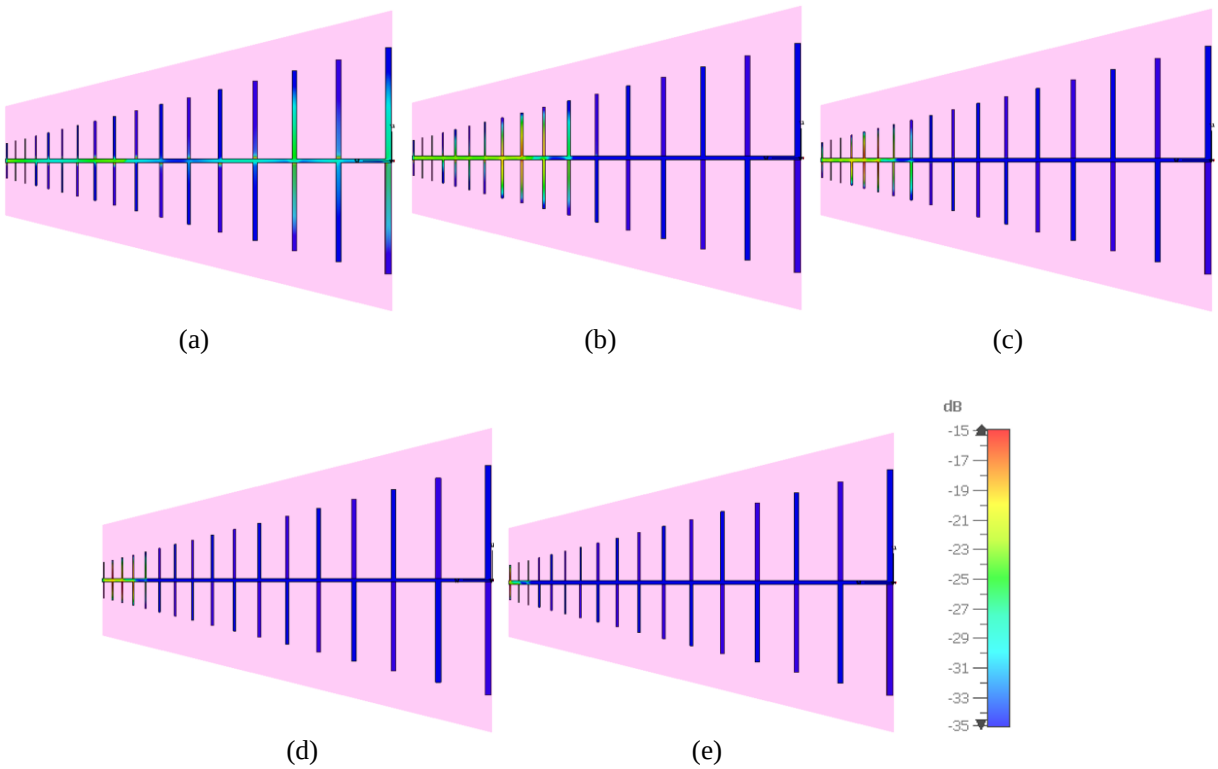

Figure 7. Current distribution on the optimized LPDA. (a) 500 MHz; (b) 1000 MHz; (c) 1500 MHz; (d) 2000 MHz; (e) 2500 MHz.

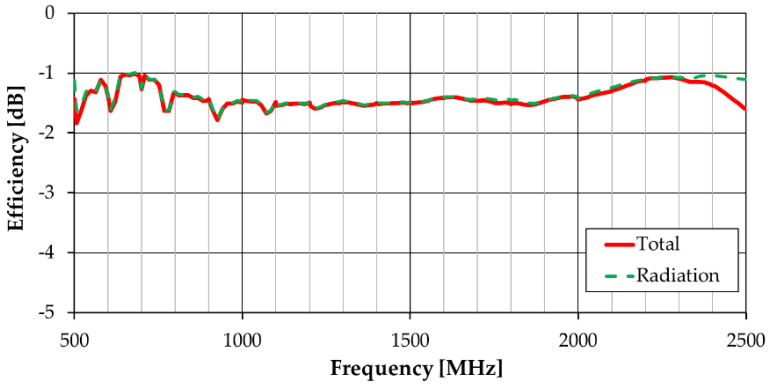

Figure 8. Efficiency simulated results of the optimized LPDA.

two orthogonal linearly polarized components are measured separately. A summary of the simulation results is shown in Table 1.

4. EXPERIMENTAL RESULTS

A prototype of the optimized LPDA has been fabricated and tested. Photographs of the prototype are shown in Fig. 10. Top side and bottom side views, as well as zooms of the feed balun, are provided. As can be seen, the cable has been soldered along the top strip of the feeding transmission line.

The experimental input reflection coefficient ($|S_{11}|$), gain, and radiation pattern results are shown in Figures 11, 6, and 13, respectively. There is a general good agreement between numerical simulation

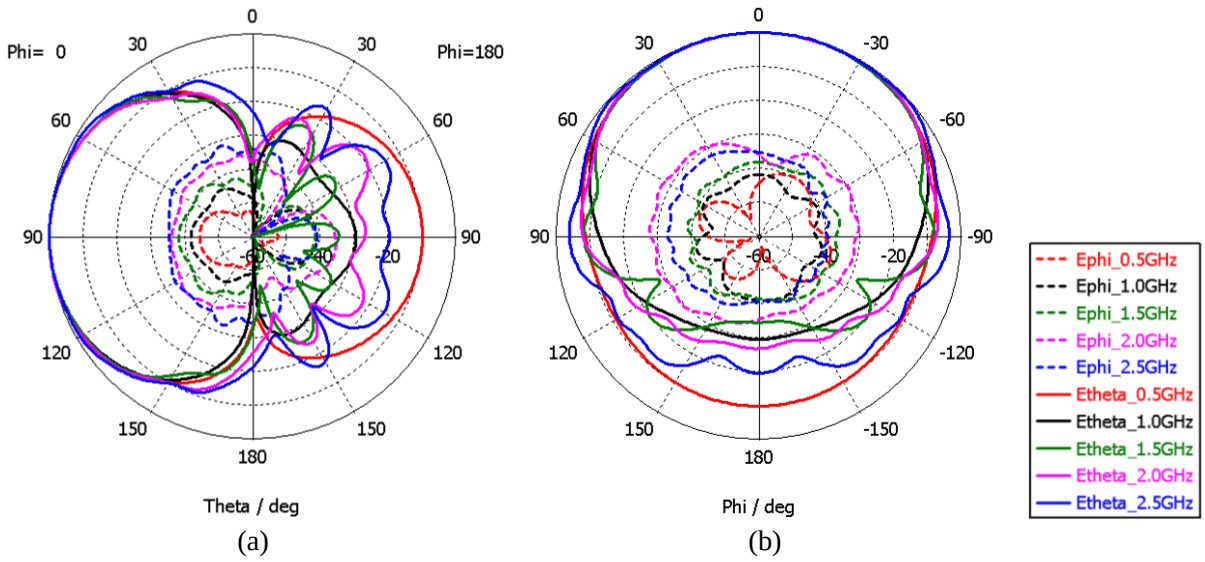

Figure 9. Radiation pattern simulated results, with polarization discrimination, of the optimized LPDA. (a) E-plane; (b) H-plane.

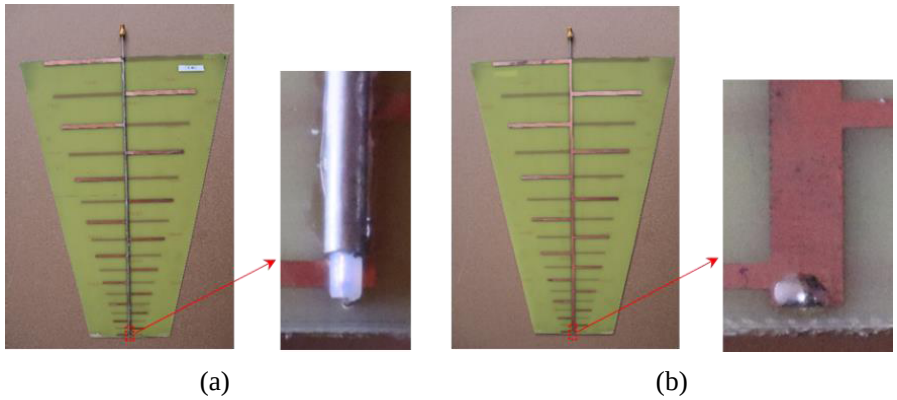

Figure 10. Photographs of the LPDA prototype. (a) Front view; (b) Back view.

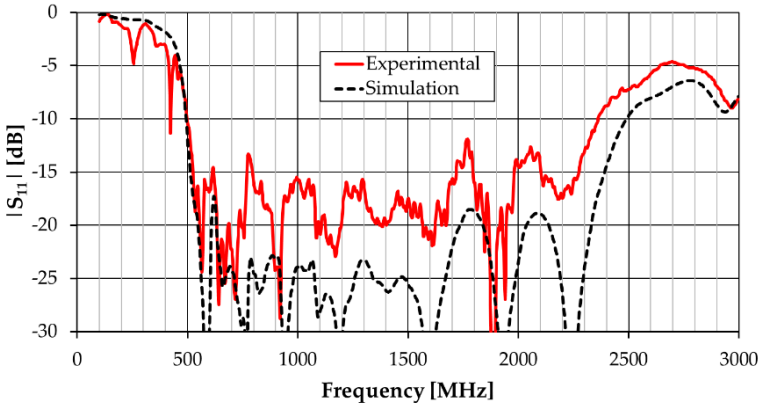

Figure 11. Comparison of simulation and experimental input reflection coefficient results (reference to 50 Ω).

and experimental $|S_{11}|$ results. However, in the frequency band of operation the experimental results are significantly above (roughly 5 to 10 dB) the simulation ones. This is mainly due to the reflections in the laboratory environment as the measurement was made outside the anechoic chamber. Moreover, there is a deterioration of the input reflection coefficient near 2.5 GHz caused mainly by minor fabrication inaccuracies of the feeding balun. Nonetheless, the reflected power is still at an acceptable level (worst case of about 18% at 2.5 GHz). Radiation pattern and gain have been measured in the far-field anechoic chamber facility of the Polytechnic University of Madrid (UPM) (Fig. 12).

The radiation pattern and gain measurements could only be taken starting at 660 MHz. The gain simulation and experimental curves have the same shape and span about the same interval (4.6–7.3 dBi). However, the experimental curve has an average of 6.6 dBi, which is 0.5 dBi above the average of the simulation one.

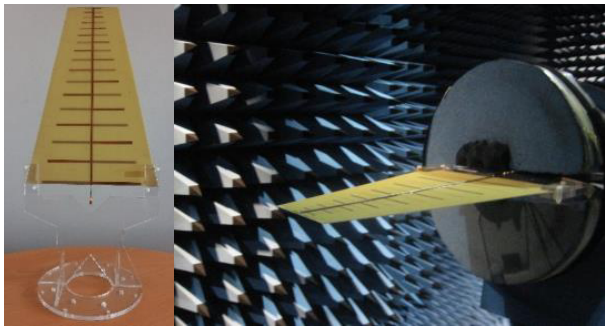

Figure 12. Photo of the antenna prototype. (a) Mounted on anacrylic interface; (b) Inside the UPM anechoic chamber.

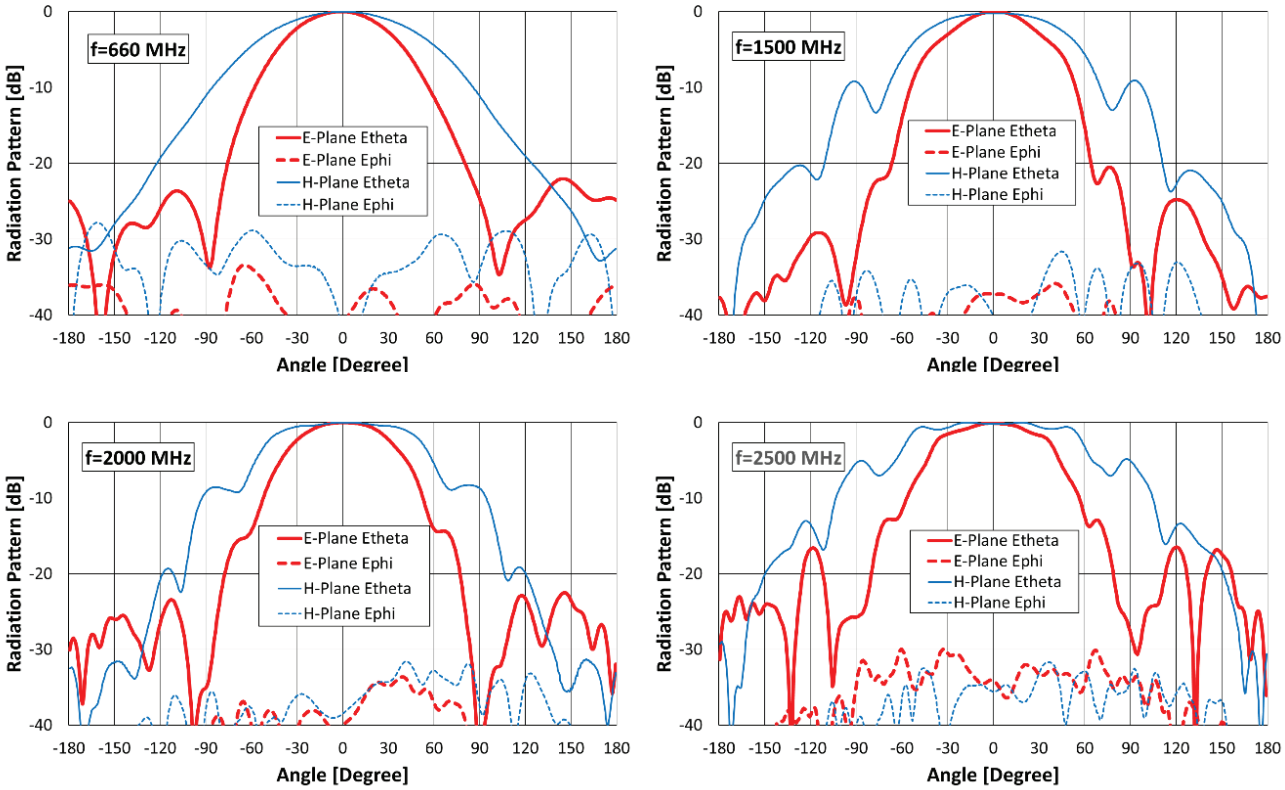

Figure 13. Experimental radiation pattern results.

From the experimental results, shown in Fig. 13, it can also be confirmed that the radiation characteristics associated with the radiation pattern are quite stable in the frequency band of operation. Moreover, it can be concluded that the simulation results, shown in Fig. 5 and Fig. 9, have a good agreement with experimental ones.

Table 1 contains the comparison of the main simulated and experimental results. When comparing the results at the low frequency limit, one must bear in mind that it was not possible to measure the radiation pattern at 500 MHz but only at 660 MHz. Moreover, the efficiency could not be measured, and consequently the corresponding experimental results are not available (NA).

Table 1. Overall comparison of simulation and experimental results.

Freq [MHz]		**500**		**1000**		**1500**		**2000**		**2500**	
Type of Result		Sim	Exp	Sim	Exp	Sim	Exp	Sim	Exp	Sim	Exp
$\|S_{11}\|$ **[dB]**		−11.7	−10.3	−23.9	−15.7	−24.4	−17.5	−23.6	−14.4	−9.8	−7.2
HPBW [Deg]	**E-Plane**	67.9	66.4*	68.3	66.6	69.3	60.4	71.4	67.1	80.6	77.8
	H-Plane	107.2	99.9*	106.9	106.7	105.6	97.5	108.3	104.3	124.6	117.6
FBR [dB]		10.0	25.0*	29.3	34.9	33.9	37.7	26.4	30.1	19.6	31.3
Cross-Pol [dB]**		−44.3	−41.4*	−41.8	−52.4	−38.2	−37.3	−36.0	−40.1	−35.3	−34.1
Rad Eff [dB]		−1.1	NA	−1.4	NA	−1.5	NA	−1.4	NA	−1.1	NA
Gain [dBi]		5.0	7.3*	6.4	7.1	6.4	7.2	6.1	6.7	4.6	4.7

* Frequency = 660 MHz

** Defined as $|E_\varphi/E_\theta|$ in the direction of maximum radiation

There is a general good agreement between CST numerical simulated and experimental results. That is the case for input reflection coefficient, half-power beamwidth (HPBW), in E-plane and H-plane, cross-polarization level, and gain. One exception is the front to back ratio (FBR) that has a very significant difference (can be more than 10 dB). However, as shown in Fig. 12, the experimental back radiation is strongly affected by the blockage of the large antenna under test positioner, and therefore, the measured FBR is not reliable.

5. CONCLUSIONS

The development of a printed log-periodic dipole antenna is presented. The design is size constrained by the photolithography printed circuit fabrication process. Good impedance matching to the 50 Ohm coaxial feeding cable and maximal gain is required in the frequency range 500–2500 MHz. The design procedure follows an iterative method where the first iteration corresponds to the free space configuration. Then, the next iterations take into account the influence of all the printed antenna physical parameters, namely: length of dipoles, inter-elements spacing, number of dipoles, asymmetric feeding line strips, width of dipoles, and substrate shape. The optimized configuration has been fabricated, printed on a low cost FR4 substrate, and tested. $|S_{11}| < -10$ dB in the frequency range 500–2362 MHz, average gain 6.6 dBi, and end-fire cross polarization level below −34 dB have been obtained. Moreover, a general good agreement has been obtained between CST Studio Suite numerical simulations and experimental results. Such good agreement has validated the proposed analysis and design procedure. These results are adequate for the envisaged application as standard antenna in simple far-field anechoic chamber antenna measurements. Taking into account the dimensions of the anechoic chamber ($8 \times 4 \times 4\,\mathrm{m}^3$) and the distance between the standard gain antenna and the antenna under test (5 m), the LPDA gain for the angle of incidence corresponding to the point of diffuse reflection at the absorber lateral walls, ceiling, and floor (38.7 degree) is, in average, 4.1 dB below the maximum. A pair of these LPDAs will be part of the standard gain antennas set, for low frequency anechoic chamber measurements at Instituto Superior Técnico, University of Lisbon. The 500 MHz superposition (2.0–2.5 GHz) of the conventional standard gain horns with the new LPDA pair allows validation of the experimental results obtained with the latter.

ACKNOWLEDGMENT

The authors warmly thank Carlos Brito for the fabrication of the prototype, the Laboratorio de Ensayo e Homologación de Antenas, of the Polytechnic University of Madrid, for the radiation pattern measurements, and Prof. João M. Felício for the support in the final CST simulations. This work was funded by Instituto Superior Técnico, Instituto de Telecomunicações and Fundação para a Ciência e a Tecnologia (FCT) under Grant UIDB/50008/2020.

REFERENCES

1. Isbell, D. E., "Log periodic dipole arrays," *IRE Transactions on Antennas and Propagation*, Vol. 8, No. 3, 260–267, 1960, doi: 10.1109/TAP.1960.1144848.
2. Carrel, R. L., "Analysis and design of the log-periodic dipole antenna," PhD Thesis, University of Illinois, USA, 1961.
3. Smith, C. E., *Log-periodic Antenna Design Handbook*, Smith Electronics Inc., Cleveland, USA, 1966.
4. Baek, Y.-H., L. H. Truong, S.-W. Park, S.-J. Lee, Y.-S. Chae, E.-H. Rhee, H.-C. Park, and J.-K. Rhee, "94-GHz log-periodic antenna on GaAs substrate using air-bridge structure," *IEEE Antennas and Wireless Propagation Letters*, Vol. 8, 909–911, 2009, doi: 10.1109/LAWP.2009.2025523.
5. Saleem, M. K., H. Vettikaladi, M. A. S. Alkanhal, and M. Himdi, "Lens antenna for wide angle beam scanning at 79 GHz for automotive short range radar applications," *IEEE Transactions on Antennas and Propagations*, Vol. 65, No. 4, 2041–2046, 2017, doi: 10.1109/TAP.2017.2669726.
6. Cui, X., G. Chen, J. Huang, H. Song, and W. Gong, "Design and application of Wuhan Ionospheric Oblique Backscattering Sounding System with the Addition of an Antenna Array (WIOBSS-AA)," *Sensors*, Vol. 16, No. 6, 887–900, 2016, doi: 10.3390/s16060887.
7. Mistry, K. K., P. I. Lazaridis, Z. D. Zaharis, I. P. Chochliouros, T. H. Loh, I. P. Gravas, and D. Cheadle, "Optimization of log-periodic TV reception antenna with UHF mobile communications band rejection," *Electronics*, Vol. 9, No. 11, 1830–1841, 2020, doi: 10.3390/electronics9111830.
8. Liu, A. and J. A. Lu, "UHF deployable log periodic dipole antenna: Concept, design, and experiment," *IEEE Transactions on Antennas and Propagation*, Vol. 69, No. 1, 538–543, 2021, doi: 10.1109/TAP.2020.3004986.
9. Ávila-Navarro, E., J. A. Carrasco, and C. Reig, "Dual printed antenna for Wi-Fi applications," *IEEE Antennas and Wireless Propagation Letters*, Vol. 8, 596–598, 2009, doi: 10.1109/LAWP.2009.2023542.
10. Casula, G. A., P. Maxia, G. Mazzarella, and G. Montisci, "Design of a printed log-periodic dipole array for ultra-wideband applications," *Progress In Electromagnetics Research C*, Vol. 38, 15–26, 2013.
11. Xu, Q.-X., X.-R. Li, and M. Ye, "High-gain printed log-periodic dipole array antenna with parasitic cell for 5G communication," *IEEE Transactions on Antennas and Propagation*, Vol. 65, No. 12, 6338–6344, 2017, doi: 10.1109/TAP.2017.2723916.
12. Wakabayashi, R., K. Shimada, H. Kawakami, and G. Sato, "Circularly polarized log-periodic dipole antenna for EMI measurements," *IEEE Transactions on Electromagnetic Compatibility*, Vol. 41, No. 2, 93–99, 1999, doi: 10.1109/15.765096.
13. Bolli, P., F. Messina, T. Pisanu, and C. Riminesi, "High-performance log-periodic dipole-antenna for radio frequency interference monitoring system at the sardinia radio telescope," *Microwave and Optical Technology Letters*, Vol. 51, No. 1, 132–136, 2009, doi: 10.1002/mop.23997.
14. Rodriguez, V., "Measurement and computational analysis of the radiation patterns of EMC antennas used in radiated-emissions measurements," *IEEE Antennas and Propagation Magazine*, Vol. 53, No. 4, 103–112, 2011, doi: 10.1109/MAP.2011.6097298.

15. Hsu, H.-T. and T.-J. Huang, "A Koch-shaped Log-Periodic Dipole Array (LPDA) antenna for universal Ultra-High-Frequency (UHF) Radio Frequency Identification (RFID) handheld reader," *IEEE Transactions on Antennas and Propagation*, Vol. 61, No. 9, 4852–4856, 2013, doi: 10.1109/TAP.2013.2264451.
16. Viswanadham, C., "A practical approach for controlling the shape of the radiation pattern of a microwave log-periodic antenna for wideband applications," *IEEE Antennas and Propagation Magazine*, Vol. 56, No. 5, 304–314, 2014, doi: 10.1109/MAP.2014.6971971.
17. Yeo, J. and J.-I. Lee, "Miniaturized LPDA antenna for portable direction finding applications," *ETRI Journal*, Vol. 34, No. 1, 118–121, 2012, doi: 10.4218/etrij.12.0211.0178.
18. Oliveira, J. G. D., J. G. Duarte Junior, E. N. M. G. Pinto, V. P. S. Neto, and A. G. D'Assunção, "A new planar microwave sensor for building materials complex permittivity characterization," *Sensors*, Vol. 20, No. 6, 6328–6342, 2020, doi: 10.3390/s20216328.
19. Vyas, R. J., B. B. Cook, Y. Kawahara, and M. M. Tentzeris, "E-WEHP: A battery-less embedded sensor-platform wirelessly powered from ambient digital-TV signals," *IEEE Transactions on Microwave Theory and Techniques*, Vol. 61, No. 6, 2491–2505, 2013, doi: 10.1109/TMTT.2013.2258168.
20. Hidaka, N., H. Sugama, A. Tsuchiya, T. Ishida, and O. Hashimoto, "Relationship between directional patterns and the electrode structure of the log-periodic dipole antenna arrays for sensitive optical electric field sensors," *Microwave and Optical Technology Letters*, Vol. 58, No. 9, 2124–2129, 2016, doi: 10.1002/mop.29992.
21. Yang, J., M. Pantaleev, P.-S. Kildal, and L. Helldner, "Design of compact dual-polarized 1.2–10 GHz eleven feed for decade bandwidth radio telescopes," *IEEE Transactions on Antennas and Propagation*, Vol. 60, No. 5, 2210–2218, 2012, doi: 10.1109/TAP.2012.2189732.
22. Bolli, P., L. Mezzadrelli, J. Monari, F. Perini, A. Tibaldi, G. Virone, M. Bercigli, L. Ciorba, P. D. Ninni, M. G. Labate, V. G. Loi, A. Mattana, F. Paonessa, S. Rusticelli, and M. Schiaffino, "Test-driven design of an active dual-polarized log-periodic antenna for the square kilometre array," *IEEE Open Journal on Antennas and Propagation*, Vol. 1, 253–263, 2020, doi: 10.1109/OJAP.2020.2999109.
23. Campbell, C. K., I. Traboulay, M. S. Suthers, and H. Kneve, "Design of a stripline log-periodic dipole antenna," *IEEE Transactions on Antennas and Propagation*, Vol. 25, No. 5, 718–721, 1977, doi: 10.1109/TAP.1977.1141653.
24. https://flann.com/wp-content/uploads/2016/01/Series-240.pdf (accessed on 21-02-2023).
25. Peixeiro, C., "Design of log-periodic dipole antennas," *IEE Proceedings H (Microwaves, Antennas and Propagation)*, Vol. 135, No. 2, 98–102, 1988, doi: 10.1049/ip-h-2.1988.0022.
26. https://www.3ds.com/products-services/simulia/products/cst-studio-suite/ (accessed on 21-02-2023).
27. Yu, L., S. Chai, H. Huang, L. Ding, K. Xiao, and F. Zhao, "A printed log-periodic dipole antenna with balanced feed structure," *2016 Progress In Electromagnetic Research Symposium (PIERS)*, 2035–2038, Shanghai, China, Aug. 8–11, 2016.
28. Constantin, A. and R. D. Tamas, "Evaluation and impact reduction of common mode currents on antenna feeders in radiation measurements," *Sensors*, Vol. 20, No. 14, 3893–3906, 2020, doi: 10.3390/s20143893.
29. Pantoja, M. F., A. R. Bretones, F. G. Ruiz, S. G. Garcia, and R. G. Martín, "Particle-swarm optimization in antenna design: optimization of log-periodic dipole arrays," *IEEE Antennas and Propagation Magazine*, Vol. 49, No. 4, 34–47, 2007, doi: 10.1109/MAP.2007.4385594.
30. Lazaridis, P. I., E. N. Tziris, Z. D. Zaharis, T. D. Xenos, J. P. Cosmas, P. B. Gallion, V. Holmes, and I. A. Glover, "Comparison of evolutionary algorithms for LPDA antenna optimization," *Radio Science*, Vol. 51, 1377–1384, 2016, doi: 10.1002/2015RS005913.
31. Li, Q.-Q., Q.-X. Xu, Y.-L. Chang, and J. Dong, "Tri-objective compact log-periodic dipole array antenna design using MOEA/D-GPSO," *IEEE Transactions on Antennas and Propagation*, Vol. 68, No. 4, 2714–2723, 2020, doi: 10.1109/TAP.2019.2949705.

32. Bantin, C. C. and K. G. Balmain, "Study of compressed log-periodic dipole antennas," *IEEE Transactions on Antennas and Propagation*, Vol. 18, No. 2, 195–203, 1970, doi: 10.1109/TAP.1970.1139650.
33. Hilbert, M., M. A. Tilston, and K. G. Balmain, "Resonance phenomena of log-periodic antennas: Characteristic-mode analysis," *IEEE Transactions on Antennas and Propagation*, Vol. 37, No. 10, 1224–1234, 1989, doi: 10.1109/8.43530.
34. Balmain, K. G. and J. N. Nkeng, "Asymmetry phenomenon of log-periodic dipole antennas," *IEEE Transactions on Antennas and Propagation*, Vol. 24, No. 4, 402–410, 1976, doi: 10.1109/TAP.1976.1141380.
35. Yang, J., "Periodicity of the input impedance of log-periodic array antennas," *IET Microwaves, Antennas & Propagation*, Vol. 6, No. 10, 1117–1122, 2012, doi: 10.1049/iet-map.2011.0599.
36. McLean, J. S., "Asymmetry in log-periodic dipole antennas and hybrid antennas due to the infinite balun," *IEEE International Symposium on Electromagnetic Compatibility & Signal/Power Integrity*, 67–72, Reno, USA, 2020, doi: 10.1109/EMCSI38923.2020.9191638.
37. Trinh-Van, S., "A low-profile high-gain and wideband log-periodic meandered dipole array with a cascaded multi-section artificial magnetic conductor structure," *Sensors*, Vol. 19, No. 20, 4404–4415, 2019, doi: 10.3390/s19204404.